

## Inelastic behavior and fracture of high modulus polymeric fiber bundles at high strain-rates

D.L. Languerand<sup>a</sup>, H. Zhang<sup>b</sup>, N.S. Murthy<sup>c,\*</sup>, K.T. Ramesh<sup>b</sup>, F. Sansoz<sup>a</sup>

<sup>a</sup> School of Engineering, University of Vermont, Burlington, VT 05405 USA

<sup>b</sup> Department of Mechanical Engineering, Johns Hopkins University, Baltimore, MD 21218 USA

<sup>c</sup> New Jersey Center for Biomaterials, Rutgers University, Piscataway, NJ 08854 USA

### ARTICLE INFO

#### Article history:

Received 7 April 2008

Received in revised form 9 September 2008

Accepted 22 September 2008

#### Keywords:

High strain-rate

Deformation

Fracture

Fibers

Kevlar®

Spectra®

### ABSTRACT

The tensile behavior and fracture mechanisms of poly(phenylene terephthalamide) (PPTA) and high modulus polyethylene (HMPE) fiber bundles were studied at high strain-rates using a tension Kolsky bar. For all fiber bundles investigated, a significant amount of strain energy was found to be dissipated by inelastic processes in addition to that due to fracture. The differences in microstructure and properties between the fibers were shown to have a noticeable influence on the inelasticity and fracture behavior in PPTA fiber bundles. No significant strain-rate effect on inelastic behavior and maximum strength was found in HMPE fiber bundles. Scanning electron micrographs of the fracture surfaces of PPTA fiber showed that the failure occurs mainly by fibrillation resulting in pointed breaks, and showed no fundamental difference in fracture mechanism at quasi-static and high strain-rates. However, the fracture mechanism in the HMPE fiber was different at quasi-static and high strain-rates, crazing was dominant at high strain-rates and plate formation under quasi-static conditions. This difference was more substantial in HMPE fibers with lower degree of crystalline order, which suggested that the inelastic behavior is governed by a precise mechanism of load transfer between the crystalline and amorphous phases present in HMPE fibers as a function of loading rate. At high strain-rates, HMPE fibers appear to be able to dissipate more strain energy than PPTA fibers due to this intrinsic change of deformation mechanism. Our results also support the idea that the mechanical behavior of a PPTA fiber bundle is inherently statistical including variations in strength distribution and alignment of the individual filaments.

© 2008 Elsevier B.V. All rights reserved.

### 1. Introduction

The specific tensile strengths of high-performance fibers produced from poly(phenylene terephthalamide) (PPTA) and high modulus polyethylene (HMPE) exceed that of steel, and appear to dissipate large amounts of energy during ballistic impact. These two fibers are marketed commercially, for example PPTA as Kevlar® (DuPont) and HMPE as Spectra® (Honeywell), respectively. Although the structure of these fibers is now well-characterized [1,2], the relationship between microstructure and macroscopic mechanical behavior is not fully understood. In particular, there is little literature on the correlation between morphology and fracture behavior in these polymers at high strain-rates. In this study, we attempt to characterize the strain-rate dependence of the tensile strength and fracture of PPTA and HMPE fiber bundles, and explore the underlying deformation mechanisms at high strain-

rates. The strain-rates  $\sim 200\text{--}1500\text{ s}^{-1}$ , which are estimated to be present when a projectile at  $\sim 500\text{ Km/h}$  hits, for instance, a planar plain-woven fabric [3,4], are readily attainable in a Kolsky bar apparatus [5].

Both PPTA and HMPE are highly crystalline. The chemical formula for the PPTA monomer is shown in Fig. 1a. Molecules including aromatic structures or amide groups are usually strong; PPTA contains both. The aramid chains form rigid planar sheets with the chain-extended molecules hydrogen bonded together. The sheets are stacked to form a crystalline array but there is only weak van der Waals forces between the sheets, which are arranged in a radial system of axially pleated lamellae as illustrated in Fig. 1b [6,7]. Microscopic, scattering and spectroscopic techniques have been extensively used to study the radial orientation of PPTA fibers [1]. The structure of pedigreed PPTA fibers (including Kevlar® 149, Kevlar® 49 and Kevlar® 29) is known to be radial lateral with crystallinity of the order of 90–95% for Kevlar® 149 and Kevlar® 49 and 80–85% for Kevlar® 29 [6]. Using wide angle X-ray diffraction, it was found that PPTA forms orthorhombic crystals with two chains per unit cell. The apparent crystallite size is 50 nm, 4.4 nm

\* Corresponding author. Tel.: +1 732 445 0488; fax: +1 732 445 0285.  
E-mail address: [murthy@biology.rutgers.edu](mailto:murthy@biology.rutgers.edu) (N.S. Murthy).

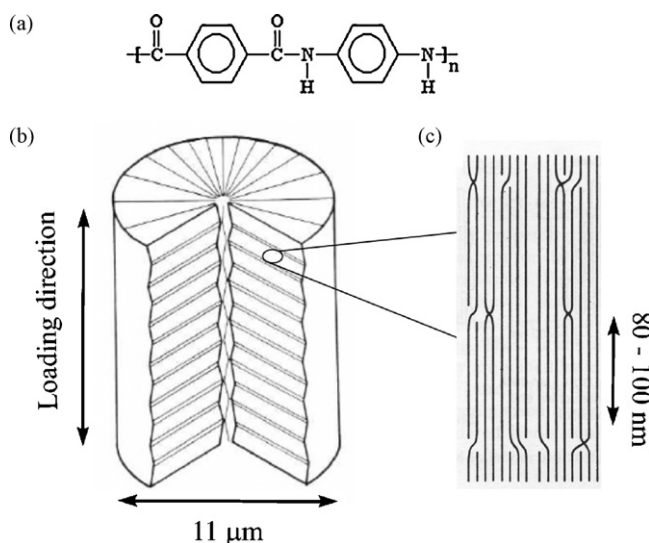


**Fig. 1.** (a) Chemical formula of PPTA; (b) radial pleated-sheet structure of PPTA filaments and (c) crystalline structure model of PPTA [1].

and 3.6 nm along [002], [1 1 0] and [2 0 0] directions, respectively. PPTA fibers have high degrees of axial and lateral crystalline order [1]. These fibers are formed by a dry-jet wet spinning process that produces liquid crystalline domains with chains oriented along the flow direction [7]. As a result, PPTA shows anisotropy in mechanical behavior with larger modulus and strength along the longitudinal orientation of the fiber.

Based on experimental data and simulation on single filaments, Cheng et al. [8] have observed that the tensile response of Kevlar<sup>®</sup> KM2 fibers is linear and elastic until failure. This behavior was related to fibrillation, i.e. decohesion of fibrils along the longitudinal axis of the fiber. The mechanical behavior was also found to be nonlinear along the transverse direction. Both longitudinal and transverse behavior showed no strain-rate dependency. In contrast, Wang and Xia [9] found a strain-rate dependence of mechanical behavior in Kevlar<sup>®</sup> 49 bundles investigated at strain-rates between  $0.0001 \text{ s}^{-1}$  and  $1350 \text{ s}^{-1}$ . Using a Weibull failure analysis, these authors have observed that the Young's modulus and strength of the fiber bundles increase slightly with increasing strain-rate. However, Creasy [10] has argued that the effects of slack and variability in test procedure may account for the apparent strain-rate dependence of these parameters.

The chemical formula for the monomer of a HMPE fiber is shown in Fig. 2a. This polymer is processed by gel spinning followed by drawing to produce longitudinally oriented chains [2]. In the gel state, polyethylene is amorphous, and the undrawn fiber is characterized by the formation of crystalline spherulites in an amorphous matrix. During drawing, the spherulites deform into parallel plate-like structures [11]. HMPE fibers usually have a lower degree of X-ray crystallinity ( $\sim 75\%$ ) than PPTA [2]. The microstructure of HMPE filaments is schematically represented in Fig. 2b. The drawn fibers consist of microfibrils and intrafibrillar matter. The microfibrils are composed of crystalline and amorphous regions oriented along the fiber axis. The aligned crystalline regions are on the order of 60–400 nm in length [2]. Though intermolecular van der Waals forces between the PE chains are weak, the primary covalent bonds along the chain-axis contribute to the strength of the fiber.

Compared to PPTA, little has been published regarding the fracture of HMPE fiber. Within the fiber, the microfibrils are aligned longitudinally and linked together by the intrafibrillar chains [2]. Under tension the microfibrils can stretch through chain unfolding, giving these regions greater strength. Prevorsek et al. [3] used

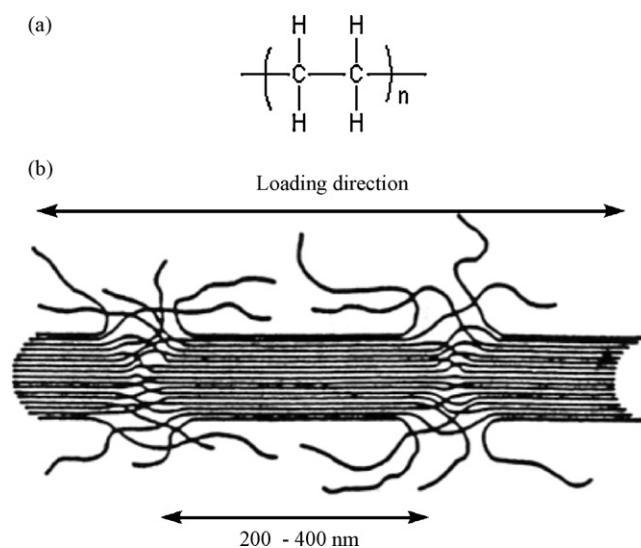


**Fig. 2.** (a) Chemical formula of HMPE and (b) longitudinal structure of HMPE microfilaments [2].

high-speed photography to observe the effects of ballistic impact on Spectra<sup>®</sup> fibers and composites. Since HMPE fibers melt at a lower temperature than PPTA, investigations of HMPE fibers have focused on heating effects in addition to deformation and failure. Another study by the same group using numerical simulation of projectile impact provided a model of heat effects during ballistic impact on polyethylene fiber composite armor [12]. It was concluded that heating effects were negligible in the armor performance of these composites.

Polyethylene is known to dissipate energy through chain unfolding and crazing in its amorphous domains, and through crystal separation and slippage in its crystalline regions [10,13]. Crazing is the primary yielding morphology seen in amorphous glassy polymers [14]. Crazes are localized zones of micro-cracking which grow perpendicular to the direction of maximum principal stress. Above the glass transition temperature, a polymer is more viscous, and thus allows energy to be absorbed through chain unfolding [15]. Because of the relatively high crystalline content, it is unclear if the same mechanisms operate in HMPE fibers.

This study describes an effort to understand the mechanical behavior and fracture of PPTA and HMPE fiber bundles under uniaxial tension at both quasi-static and high strain-rates. Atomic force microscopy (AFM) was used to characterize the cross-sectional structure of the filaments. Uniaxial tensile tests were conducted at high strain-rates using a tension Kolsky bar. The failure modes and mechanisms were investigated by scanning electron microscopy (SEM) and related to the structure of each of the fiber samples. Section 2 presents the details of the experimental procedure. The results obtained from mechanical testing and fracture surface analyses are presented in Section 3. The relationships between microstructure, mechanisms, and strain-rate dependence of deformation and fracture in PPTA and HMPE are discussed in Section 4.

## 2. Experimental

### 2.1. Materials

Three grades of PPTA fiber bundles (DuPont) labeled Fiber-A, -B and -C, were tested [16,17]. The first two types of fiber belong to the same family of PPTA, but were obtained from different processing conditions. Two HMPE fiber bundles (Honeywell) labeled Fiber-A and -B [18,19] were used in this study with the former having lower



Fig. 3. Holder used for high strain-rate tests.

crystalline order than the latter. There were about 530 filaments in PPTA (12  $\mu\text{m}$  dia.) fibers, 120 in HMPE Fiber-A (38  $\mu\text{m}$  dia.) and 240 in HMPE Fiber-B (26  $\mu\text{m}$  dia.).

## 2.2. Mechanical testing

High strain-rate tensile tests were carried out using a tension Kolsky bar [20–22]. A laser detector, consisting of a line laser emitter, optics, and a photodiode [23] was used to measure both the initial fiber length and elongation during testing. The strain-rate varied from  $340\text{ s}^{-1}$  to  $850\text{ s}^{-1}$ . In order to produce a breaking strength that was in the range of the Kolsky bar, several fiber bundles were held in place using a jig (Fig. 3) and tested in tension. The PPTA samples were glued using quick-set epoxy and clamped, while the HMPE samples were simply clamped in place. The initial fiber bundle length ranged from 3.416 mm to 4.539 mm depending on the samples.

## 2.3. Mechanical and fracture analyses

The onset of failure is assumed to occur at the peak of the stress. The filaments in the bundle did not all break simultaneously, and the strain did not drop to zero immediately after the peak stress. The total failure of the fiber bundles occurs when the stress returned to zero after the peak stress. The total strain energy dissipated was calculated by integrating the tensile stress–strain curve from zero strain to the breaking strain and by dividing this value by the material volume. The inelastic strain energy density was calculated by subtracting the elastic strain energy density from the total strain energy density. The apparent elastic modulus was determined from the linear portion of the loading curve neglecting the curvature near zero-load.

Fracture mechanisms of the fibers were investigated by examining the fractured regions using SEM observations (JEOL JSM6060). For this purpose, the fractured fibers were mounted on double-sided conductive tape and gold-sputtered in vacuum to produce a 100 nm conductive coating. Also, several tests were performed on PPTA and HMPE fiber bundles at quasi-static strain-rates using a standard materials testing machine (Instron), and the fibers were examined under SEM for comparison. Furthermore, the cross-sectional microstructure of the undeformed filaments was observed by AFM (Universal SPM Quesant) in intermittent mode using a silicon cantilever with a tip radius of 10 nm and force constant of 40 N/m (NSC16, Mikromasch). For this purpose the fiber bundle was embedded in epoxy resin, the cross-section was mechanically polished with wet sand paper up to 1200 grit, and subsequently polished with diamond pastes up to 0.25  $\mu\text{m}$ .

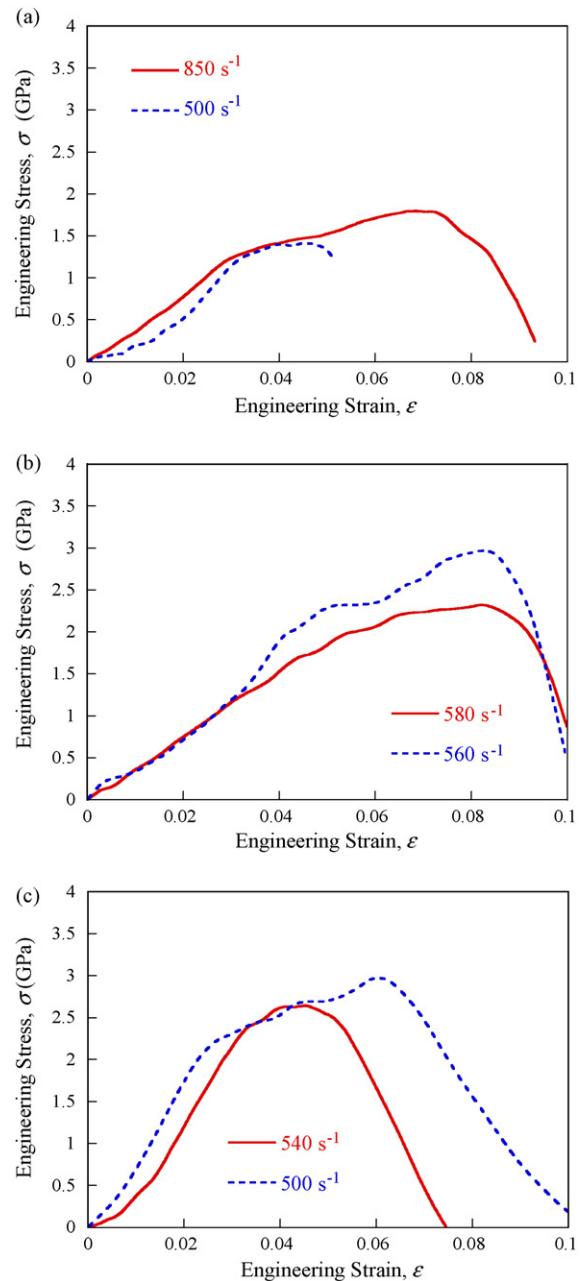


Fig. 4. Tensile behavior at quasi-static and high strain-rates of (a) PPTA Fiber-A, (b) PPTA Fiber-B and (c) PPTA Fiber-C.

## 3. Results

The mechanical parameters determined from the tensile stress–strain curves at high strain-rates on PPTA and HMPE fiber bundles are shown in Tables 1 and 2, respectively. These parameters are used to understand the differences in the performance of the three PPTA fibers and the two HMPE fibers used for this study. In the tests with Kolsky apparatus, the number of wave reverberations within the sample before failure was found to be between 4 and 7 for all the tests reported here. Thus the fiber bundles can be assumed to have reached dynamic equilibrium by the time the specimen begins to fail. Even though the modulus obtained at high strain-rates in this study may not be reliable, the strength and the energy absorbed are meaningful.

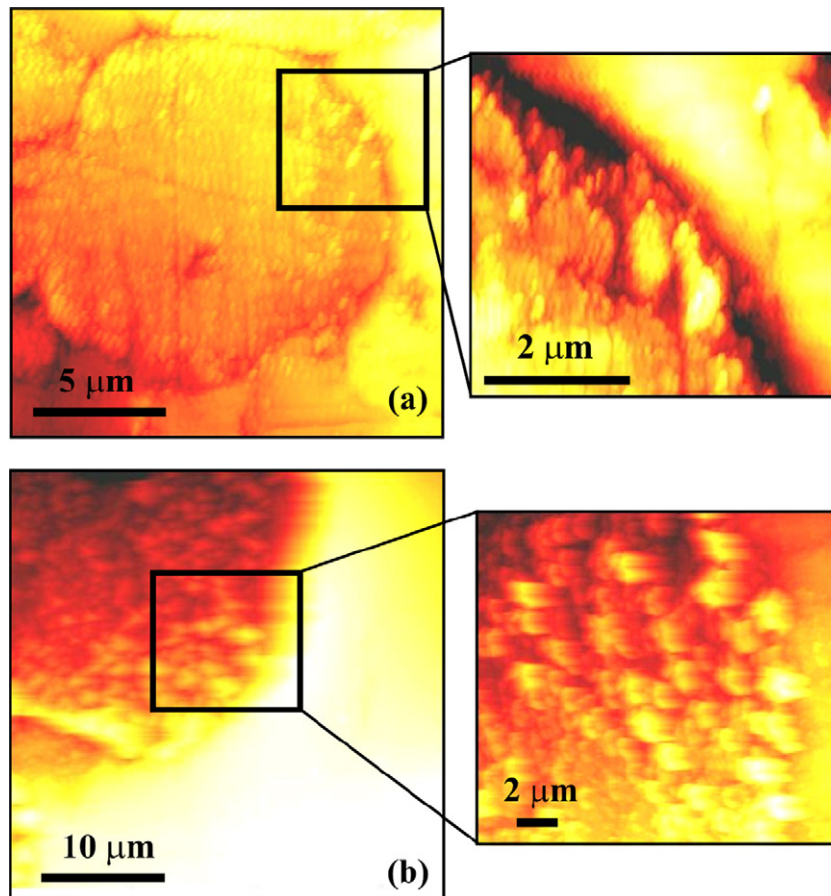


Fig. 5. Intermittent-mode AFM micrographs of (a) PPTA 29 (1) and (b) HMPE Fiber-A.

### 3.1. PPTA fiber bundles

#### 3.1.1. Tensile mechanical behavior

The tensile stress–strain curves in PPTA fiber bundles deformed at different strain-rates are presented in Fig. 4 and the analysis is summarized in Table 1. Fibers A and B belong to the same family as Kevlar® 49 and 29, respectively. Based on this similarity, and drawing from the published literature, we can conclude that A and B have lower degree of crystallinity and orientation than C [6]. This leads us to conclude that for the PPTA bundles tested, the apparent modulus determined appears to be strongly influenced by the fiber morphology (combination of crystallinity, crystalline order and orientation) and the strain-rate. The moduli at high strain-rates are lower than the quasi-static values reported in the literature [8]. The influence of microstructure on the tensile strength in these fibers is small.

All the PPTA fiber bundles broke in high strain-rate tests. Fiber-B and Fiber-C dissipated more inelastic strain energy than Fiber-A during deformation at all strain-rate. Therefore, there is a strong microstructure dependence in terms of inelastic behavior and fracture. In addition, as shown in Tables 1 and 2, the breaking strain corresponding to the complete failure is between 5% and 11%, which is greater than the value reported in the literature on single filaments. This is likely a consequence of stochastic failure process, as discussed below.

#### 3.1.2. Microscopy and fracture mechanisms

Fig. 5a presents the cross-sectional AFM images of PPTA Fiber-A obtained from intermittent contact mode. The radial structure of

PPTA [6] is not readily apparent in this figure. However, the view at a higher magnification suggests that the structure of the skin and core regions of the cross-section do differ. In this material, earlier nano-indentation studies have found that the skin structure possesses different mechanical properties than the core [24]. Furthermore, features suggesting a submicron scale structure corresponding to the fibrillar morphology of the fiber can be seen in the micrographs.

The predominance of a fracture mechanism in a particular fiber under given condition was investigated statistically via SEM analysis. Table 3 summarizes the statistical distribution of each of the fracture mechanisms observed in all the SEM micrographs. Under tension, PPTA fibers show three types of fracture morphology: fibrillated break, pointed break and breaks with transverse striations. Fibrillation, which is most common, is characterized by decohesion, a reduction in diameter and splintering of the microfibrils along the longitudinal axis of the fiber and the fracture surfaces has a bamboo-like appearance (Fig. 6). Pointed break, frequently seen when filaments fail at slow strain-rate (especially in PPTA Fiber-C), is accompanied by a significant necking and reduction in fiber diameter and tapered diameter near the fractured area, which results from significant localization of deformation in the crystalline phase of the polymer (Fig. 7). Breaks with transverse striations (Fig. 8) resemble kink-bands that are usually seen under compressive loads, and occurs when the filaments break prematurely due to the presence of dislocations in the ordered molecular chains [25] that often involve the entire microfilament. However, there is no significant influence of the strain-rate on these deformation mechanisms in all PPTA fibers tested.

**Table 1**  
Summary of results obtained on PPTA fiber bundles tested at high strain-rates.

Strain-rate ( $s^{-1}$ )	PPTA Fiber-A			PPTA Fiber-B			PPTA Fiber-C		
	Quasi-static	500	850	Quasi-static	560	580	Quasi-static	500	540
Elastic modulus (GPa)	77	59 ± 6	48 ± 3	63	41 ± 9	41 ± 7	120	99 ± 15	105 ± 14
Tensile strength (GPa)	3.4	1.57 ± 0.08	1.89 ± 0.09	3.0	2.9 ± 0.1	2.4 ± 0.1	3.1	3.8 ± 0.2	3.0 ± 0.2
Strain at tensile strength (%)		4.5	7.0		8.0	8.3		6.2	4.4
Breaking strain (%)	3.1	5.0	9.5	3.7	10.0	10.6	2.4	10.0	10.0
Dissipated strain energy density ( $J/mm^3$ )		0.0457	0.119		0.173	0.166		0.235	0.149
Inelastic strain energy density ( $J/mm^3$ )		0.032 ± 0.003	0.1052 ± 0.002		0.112 ± 0.008	0.120 ± 0.005		0.196 ± 0.005	0.061 ± 0.007

**Table 2**  
Summary of results obtained on HMPE fiber bundles tested at high strain-rates.

Strain-rate ( $s^{-1}$ )	HMPE Fiber-A			HMPE Fiber-B			
	Quasi-static	340	530	800	Quasi-static	540	670
Elastic modulus (GPa)	66	25 ± 5	40 ± 7	19 ± 3	113	33 ± 6	36 ± 3
Tensile strength (GPa)	2.40	0.96 ± 0.05	0.80 ± 0.05	1.07 ± 0.08	3.25	1.82 ± 0.09	2.03 ± 0.08
Strain at tensile strength (%)		8.9	6.8	11.1		12.0	11.1
Breaking strain (%)	4.1	14.0	12.4	19.4	2.9	19.3	19.4
Dissipated strain energy density ( $J/mm^3$ )		0.105	0.070	0.131		0.234	0.281
Inelastic strain energy density ( $J/mm^3$ )		>0.092 ± 0.004	>0.055 ± 0.004	>0.096 ± 0.006		>0.198 ± 0.003	>0.174 ± 0.004

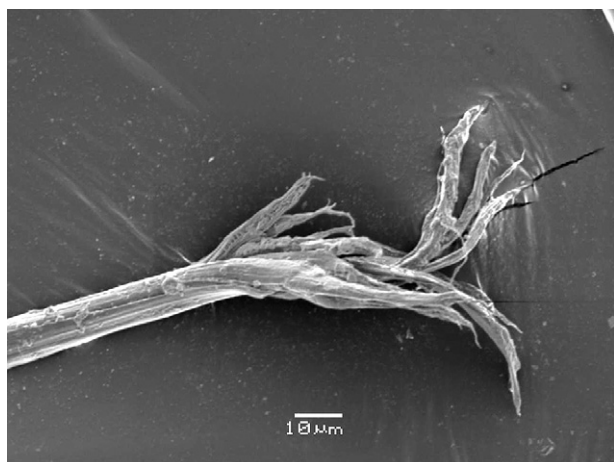


Fig. 6. SEM image showing a fibrillated break in PPTA 29 (2) failed at high strain-rate.

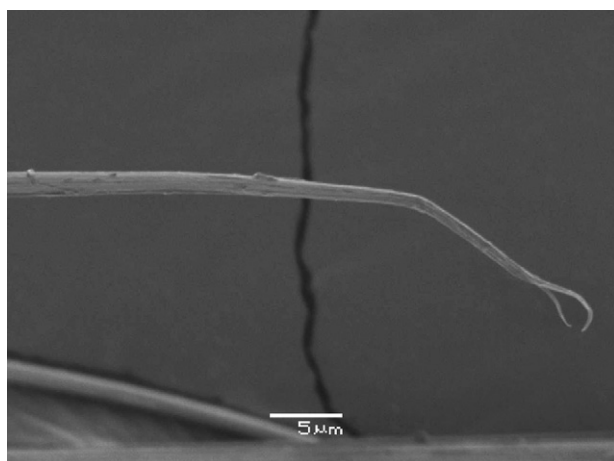


Fig. 7. SEM image showing a pointed break in PPTA Fiber-C failed at quasi-static strain-rate.

### 3.2. HMPE fiber bundles

#### 3.2.1. Tensile mechanical behavior

The tensile stress–strain curves of the HMPE fiber bundles deformed at different strain-rates are presented in Fig. 9. The anal-

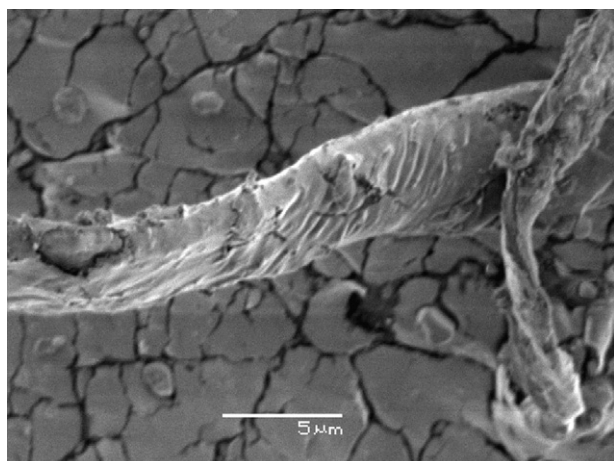


Fig. 8. SEM image showing a break accompanied by transverse striations in PPTA Fiber-A that failed at high strain-rate.

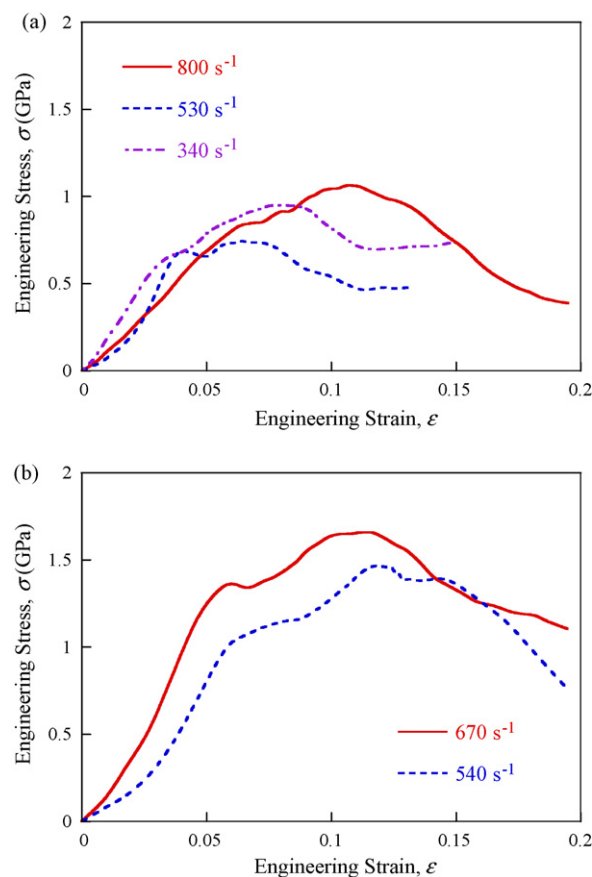


Fig. 9. Tensile behavior at quasi-static and high strain-rates of (a) HMPE Fiber-A and (b) HMPE Fiber-B.

ysis of these curves is summarized in Table 2. It has been reported that the degree of orientation and other measures of crystalline order such as crystallinity and crystallite size are higher in Fiber-B than in Fiber-A [26–28]. Thus, the data in Table 2 show that, similar to the results obtained in PPTA, some of the properties such as the strength and the dissipated strain energy in HMPE fiber bundles are more significantly influenced by the fiber morphology than the strain-rate. The moduli obtained here for HMPE at all strain-rates are smaller than those reported in the literature, perhaps due to fiber slippage. This discrepancy, however, will not alter the main conclusions concerning the modes of failure in HMPE fiber bundles.

This figure also shows that the strength of HMPE fiber bundles does not increase with strain-rate, and are perhaps lower at high strain-rates. HMPE Fiber-B fiber bundles are also markedly stronger than HMPE Fiber-A fiber bundles at all strain-rates, indicating that the inelastic behavior and fracture processes are also highly dependent on the fiber morphology. Specific strain-rate effect on the dissipated strain energy in HMPE fiber bundles could not be deduced from the data because most of the HMPE fiber bundles tested under high strain-rate loading did not break. In HMPE Fiber-B, only a limited amount of fiber (<25%) in the bundles completely failed in each of the two high strain-rate tests; none of the HMPE Fiber-A bundles failed under high strain-rate tensile loading. However, HMPE fiber bundles break at larger strain than PPTA at high strain-rates, and clearly possess a larger propensity to dissipate strain energy during deformation than PPTA fibers. The main explanation for such a difference is related to the significant energy dissipation taking place in the inelastic processes. The slower decrease of stress at the onset of failure in HMPE than in PPTA (Figs. 4 and 9) suggests that the failure mechanism in this

**Table 3**  
Statistical predominance of the fracture mechanisms observed by SEM for each material. The percentage corresponds to the occurrence of a fracture mechanism with respect to the total number of mechanisms observed on all micrographs.

Material	Strain-rate	Crazing	Fibrillation	Plate formation	Pointed break	Transverse striations
PPTA Fiber-A	High	–	68	–	23	9
	Quasi-static	–	74	–	26	–
PPTA Fiber-B	High	–	76	–	24	–
	Quasi-static	–	80	–	20	–
PPTA Fiber-C	High	–	79	–	21	–
	Quasi-static	–	54	–	46	–
HMPE Fiber-A	High	54	19	27	–	–
	Quasi-static	14	25	61	–	–
HMPE Fiber-B	High	44	21	35	–	–
	Quasi-static	31	28	44	–	–

material is different and as a result dissipate more energy than PPTA, albeit slowly.

### 3.2.2. Microscopy and fracture mechanisms

Fig. 5b presents the cross-sectional AFM images of HMPE Fiber-A obtained in intermittent mode. No specific core-skin difference in microstructure is observed in this figure. Furthermore, similar to the PPTA cross-section, a submicron scale structure, the fibrillar morphology, can be clearly observed in the close up view. It can be observed that this submicron scale structure appears to be coarser than in PPTA fibers. This observation supports the assumption that the crystalline phases are significantly smaller in size and denser in PPTA fiber bundles than HMPE fibers.

The fracture mechanisms of HMPE fibers investigated by SEM include crazing, fibrillation and plate formation. There is clear evidence of crazing at the surface of HMPE fibers in Figs. 10 and 11. Fibrillation and plate formation mechanisms can be seen in HMPE in Figs. 10 and 12, respectively. Plate formation results from slippage between the crystalline regions in the fiber matrix. This slippage results from secondary bond breakage between the ordered macromolecules as explained in the Section 4. Table 2 shows that the predominant fracture mechanism in HMPE fibers strongly depends on the strain-rate. The fibers broken at quasi-static rates are characterized predominantly by plate formation with fibrillation and to a lesser extent, crazing. At high strain-rates, however, there is

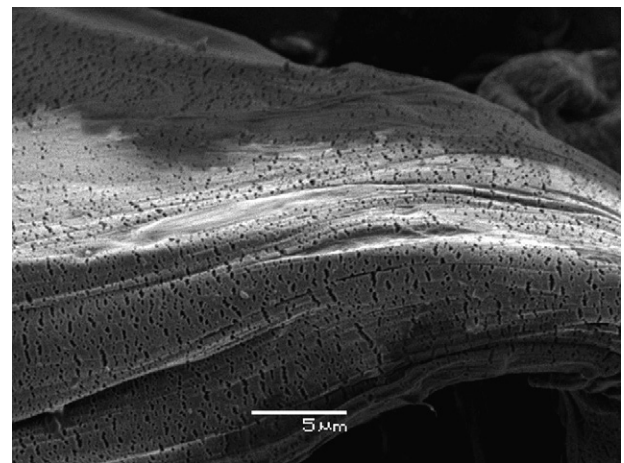


**Fig. 11.** SEM image showing extensive crazing on the surface of HMPE Fiber-A failed at high strain-rate.

a significant change of mechanism from plate formation to crazing. This effect appears to be more drastic in HMPE Fiber-A, which has a lower crystalline order than HMPE Fiber-B. Some fibrillation also appears in the HMPE fibers tested, but the occurrence of this mechanism does not appear to be influenced by the strain-rate.

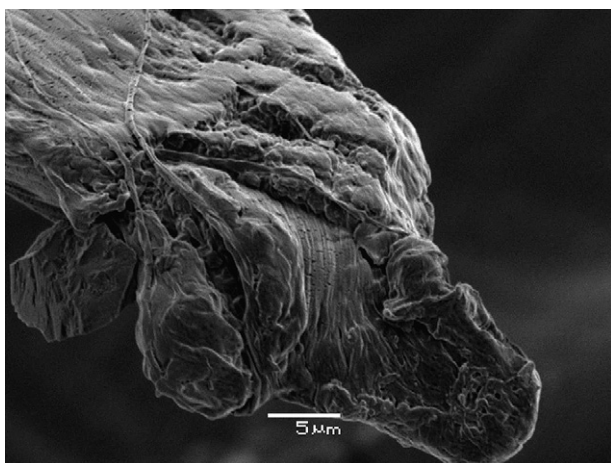


**Fig. 10.** SEM image showing fibrillated break and some crazing in HMPE Fiber-B failed at high strain-rate.

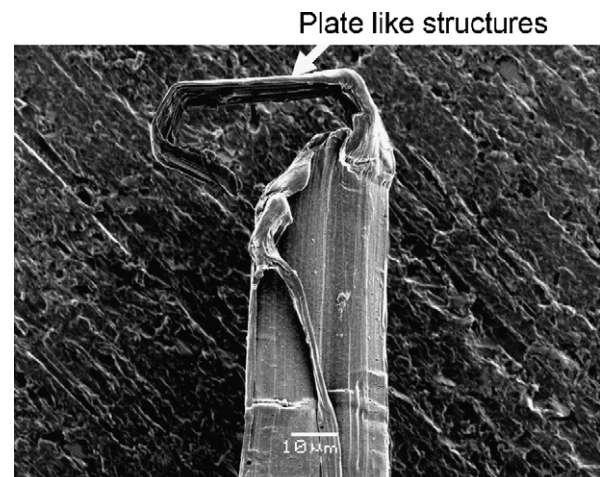


**Fig. 12.** SEM image showing a plate formation in HMPE Fiber-B failed at quasi-static strain-rate.

## 4. Discussion

The key result of this study is that the fracture processes are different at low and high strain-rates, especially in HMPE fibers. These differences most likely explain the observed difference in strength and absorbed energy in these fibers. Also, we observed that the mechanical behavior of the bundles is quite different from that of single filaments.

### 4.1. Effects of variability on fracture in high-modulus polymeric fiber bundles

Testing fiber bundles introduces an intrinsic mechanical effect as compared to experiments on single filaments [10]. Filaments in a bundle do not all have the same length or the same strength [29]. Our experiments indicate that fiber bundles have same elastic modulus as the single fibers. However, slack causes the breaking strain and inelastic strain energy density to be larger than they would otherwise be in a perfectly aligned monofilament. This can be explained as follows. When the first filaments break, the stress is likely to increase in the bundle, and is not necessarily redistributed evenly to all of the remaining filaments [13]. Therefore, filaments within bundles often fail in bursts, in which many filaments break at the same time. It is likely that the filament failure does not lead to a uniform transfer of the load to the remaining filaments; instead, load transfer may be highly localized to the filaments neighboring the fracture site.

It is important to note the difference between the results of Cheng et al. [8] on commercial PPTA fibers, Kevlar<sup>®</sup>, with those observed here on PPTA. These differences can be again interpreted from the fundamental difference of mechanical behavior between single filament and fiber bundle. These authors investigated the tensile response of single Kevlar<sup>®</sup> KM2 filaments at quasi-static and high strain-rates, while in this study a bundle of approximately 560 filaments was tested. Cheng and co-workers found no strain-rate dependence in Kevlar<sup>®</sup> KM2, and found a linear elastic behavior followed by an abrupt drop in stress at both quasi-static and high strain-rates in Kevlar<sup>®</sup> KM2. In the current study significant differences in breaking strain and inelastic strain energy dissipated during deformation were found at high strain-rates between fiber bundles of different morphology (Fig. 4). Therefore, our study reveals a strong dependence of the fracture process on fiber morphology and structure in PPTA fiber bundles. Our SEM fracture surface analysis also shows that fibrillation is the primary failure mechanism in all PPTA fibers. This result is consistent with the findings of Cheng et al. [8]. Therefore, the difference in mechanical behavior observed in PPTA is not due to an intrinsic change of deformation mechanism, but rather to the fiber bundle mechanics. These authors have also found significant variations of strength from one fiber to another, which supports the idea that the mechanical behavior of a fiber bundle is inherently statistical with respect to many parameters, including the strength distribution and alignment of the individual filaments.

### 4.2. Inelastic behavior in PPTA fiber bundles

Our results show that strain-rate has no significant effect on elastic modulus in PPTA fiber bundles. The differences in the modulus in the three fibers tested do, however, indicate that modulus is related to the fiber morphology (orientation and crystalline order). There are two possible explanations for this difference in fracture behavior at different strain-rates: first, bundle effect could be more pronounced at low strain-rates in which case the fracture is the result of the bursts of filament bundles; second, the fracture mechanism could change with strain-rate, but we observed no fun-

damental difference in deformation mechanism from quasi-static to high strain-rates for each of the PPTA fibers tested. The underlying fracture mechanisms are related to fibrillation and, to a lesser extent, pointed break regardless of the strain-rate. This implies that the intrinsic fracture mechanisms in these fibers have only a limited contribution in terms of strain energy dissipation since these mechanisms are associated with a brittle decohesion process. The change in inelastic behavior and fracture process with strain-rate in PPTA is largely accounted for on the basis of bundle mechanics effects.

### 4.3. Inelastic behavior in HMPE fiber bundles

This study shows limited strain-rate effect on maximum strength in HMPE fiber bundles. As opposed to PPTA, however, there is clear strain-rate dependency in the form of a change in fracture mechanisms from quasi-static regime to high strain-rate regime. In the two HMPE samples studied, analysis of the fracture surfaces showed that crazing is more common at high strain-rates than at quasi-static strain-rates, whereas plate formation is more often seen at quasi-static strain-rates. This trend is more substantial in the HMPE fibers with the lower crystallinity (HMPE Fiber-A). Crazing is known to occur in the amorphous region of the fibers, while plate formation is related to the slippage of the crystalline phases. It can be concluded that the absence of strong strain-rate effect on the inelastic behavior in HMPE fiber bundles results from load transfer at the microstructure-level, which involves crazing in the noncrystalline regions and plate-slippage.

We can attempt to understand the above results using the data reported in the literature on crystalline polyethylene. Using a stochastic model of failure for perfectly ordered and oriented polyethylene, Termonia et al. [30] have shown that polyethylene displays a strong strain-rate dependence of the maximum strength; higher strength was predicted at high strain-rates [30]. At high strain-rates, these authors found that polyethylene of both high and low molecular weight fails in a brittle mode and fracture is substantially accompanied by the cleavage of primary C–C bonds. They also report that failure at low strain-rates is dominated by secondary bond breakage, which are weaker than the primary bonds. In the present study, the cleavage of secondary bonds predicted by Termonia et al. [30] at low strain-rate could also be associated with the plate formation and crystal slippage observed predominantly under quasi-static condition. This hypothesis is further confirmed by the observation that fibrillation is more important in HMPE Fiber-B than HMPE Fiber-A, and at low strain-rate than high strain-rates. At high strain-rate the fracture does not easily occur within the ordered chains because the deformation, according to Termonia et al.'s study, is predominantly localized on strong primary bonds. Therefore, an alternative load transfer occurs through the amorphous regions instead of the crystalline phases. This mechanism, in turn, results in making the amorphous regions behave like a glassy polymer, leading to a higher incidence of crazing at high strain-rate as shown in Table 3. The underlying strengthening mechanism at high strain-rate could therefore be correlated to a load transfer to the amorphous regions which exhibit a viscous behavior through chain unfolding. In this process, strength in the HMPE fiber bundles at elevated strain-rates is governed by the strength of the primary bonds in the molecular chains.

## 5. Conclusions

The fracture of PPTA and HMPE fiber bundles at room temperature were studied under high strain-rate deformation using a tension Kolsky bar. The underlying fracture mechanisms were

investigated statistically by SEM analysis of the fracture surfaces. The major findings of this study are as follows.

- For all fiber bundles investigated a significant amount of strain energy was found to be dissipated during deformation due to inelastic and fracture processes.
- Fiber morphology effects were clearly evidenced on the inelastic behavior and fracture process in PPTA fiber bundles. Fracture surface examinations by SEM indicated that the main fracture mechanisms in PPTA fibers were associated with fibrillation and, to a lesser extent, pointed breaks. The difference in mechanical behavior observed from quasi-static to high strain-rates was not due to an intrinsic change of deformation mechanism, but rather to an intrinsic effect of fiber bundle mechanics. Our results support the idea that the mechanical behavior of a PPTA fiber bundle is inherently statistical including variations in strength distribution and alignment of the individual filaments.
- In HMPE fiber bundles, no significant strain-rate effect on the maximum strength was observed. As opposed to PPTA, however, there is clear evidence of a change of fracture mechanism at the single fiber level, from the quasi-static regime to the high strain-rate regime. HMPE fibers appear to dissipate more strain energy than PPTA at high strain-rates. In the two types of HMPE materials studied, analysis of the fracture surfaces showed that crazing is more common at high strain-rates than at quasi-static strain-rates, whereas plate formation is more often seen at quasi-static strain-rates. This trend is more substantial in the HMPE fibers with the lower crystallinity. It was shown that crazing is a more important energy absorbing mechanism in HMPE at high strain-rates than at quasi-static rates. Therefore, it can be concluded that the absence of the strain-rate dependence on strength and fracture in HMPE fiber bundles is predominantly linked to a precise mechanism of load transfer as a function of strain-rate from slippage of crystal plates to crazing in the crystalline regions of the HMPE fibers.

#### Acknowledgements

This work was funded by NSF grant DMR-0513926. F.S. and N.S.M. would also like to acknowledge support from NSF-Vermont Experimental Program to Stimulate Competitive Research (VT

EPSCoR) under grant number NSF EPS 0236976. We thank Dr. Nguyen of Honeywell for providing the HMPE fibers, and Dr. Gabara of DuPont for the PPTA fibers.

#### References

- [1] H.H. Yang, Kevlar Aramid Fiber, John Wiley and Sons Ltd., England, 1993.
- [2] D.C. Prevorsek, in: M. Lewin, J. Preston (Eds.), High Technology Fibers Part D, Marcel Dekker, Inc., USA, 1996, pp. 1–169.
- [3] D.C. Prevorsek, H.B. Chin, Y.D. Kwon, J.E. Field, J. Appl. Polym. Sci. 47 (1991) 45–66.
- [4] B. Gu, Composites B 34 (2003) 361–371.
- [5] B.A. Gama, S.L. Lopatnikov, J.J.W. Gillespie, Appl. Mech. Rev. 57 (2004) 223–250.
- [6] A.P. Smith, H. Ade, Appl. Phys. Lett. 69 (1996) 3833–3835.
- [7] D. Taner, J.A. Fitzgerald, P.G. Riewald, W.F. Knoff, in: M. Lewin, J. Preston (Eds.), High Technology Fibers Part B, Marcel Dekker, Inc., USA, 1989, pp. 37–39.
- [8] M. Cheng, W. Chen, T. Weerasooriya, J. Eng. Mater. Technol. 127 (2005) 197–203.
- [9] Y. Wang, Y. Xia, Composites A 29A (1998) 1411–1415.
- [10] T.S. Creasy, J. Compos. Mater. 36 (2002) 183–194.
- [11] S.Y. Lee, D.C. Bassett, R.H. Olley, J. Mat. Sci 35 (2000) 5101–5110.
- [12] D.C. Prevorsek, Y.D. Kwon, H.B. Chin, Polym. Eng. Sci. 34 (1994) 141–152.
- [13] P.C. Hemmer, A. Hansen, S. Pradhan, in: P. Bhattacharyya, B.K. Charabarti (Eds.), Modeling Critical and Catastrophic Phenomenon in Geoscience: A Statistical Physics Approach. Series: Lecture Notes in Physics 705 Springer, Berlin, 2006, pp. 27–55.
- [14] H.H. Kausch, Polymer Fracture, Springer-Verlag, Berlin/Heidelberg, 1978.
- [15] G. Strobl, The Physics of Polymers, Springer-Verlag Berlin Heidelberg, Germany, 1997.
- [16] E.I. du Pont de Nemours Co. Inc., Product information, Bulletin K-1, December 1974.
- [17] E.I. du Pont de Nemours Co. Inc., Product information, Bulletin K-5, September 1981.
- [18] Honeywell International Inc. USA, Spectra® Fiber 900, Honeywell Product Information, 2004.
- [19] Honeywell International Inc. USA, Spectra® Fiber 1000, Honeywell Product Information, 2004.
- [20] G. Cray, ASM Handbook, vol. 8, ASM International, Materials Park, OH, 2000, pp. 488–496.
- [21] D.R. Chichili, K.T. Ramesh, Int. J. Solids Struct. 32 (1995) 2609–2626.
- [22] Y. Li, K.T. Ramesh, Key Eng. Mater. 243–244 (2002) 153–158.
- [23] K.T. Ramesh, Narasimhan, Int. J. Solids Struct. 33 (1996) 3723–3738.
- [24] J.F. Graham, C. McCague, O.L. Warren, P.R. Norton, Polym. Eng. Sci. 41 (2000) 4761–4764.
- [25] H.F. Wu, J.R. Yeh, J. Mater. Sci. 27 (1992) 755–760.
- [26] Y. Fu, W. Chen, M. Pyda, D. Londono, B. Annis, A. Boller, A. Habenschuss, J. Cheng, B. Wunderlich, J. Macromol. Sci. B 35 (1996) 37–87.
- [27] N. Khosravi, S.B. Warner, N.S. Murthy, S. Kumar, J. Appl. Polym. Sci. 57 (1995) 781–787.
- [28] A. Wawkuszewski, H.-J. Cantow, S.N. Magonov, J.D. Hewes, M.A. Kocur, Acta Polymerica 46 (1995) 168–177.
- [29] S. Pradhan, B.K. Chakrabarti, Int. J. Modern Phys. B 17 (2003) 5565–5581.
- [30] Y. Termonia, P. Meakin, P. Smith, Macromolecules 19 (1986) 154–159.